IEEE Photonics Journal
An IEEE Photonics Society Publication

Open Access

Photonic Crystal Mikaelian Lenses and Their Potential Use as Transverse Focusing Elements in Microstructured Fibers

Volume 5, Number 4, August 2013

T. Baghdasaryan
T. Geernaert, Member, IEEE
H. Thienpont, Member, IEEE
F. Berghmans, Member, IEEE

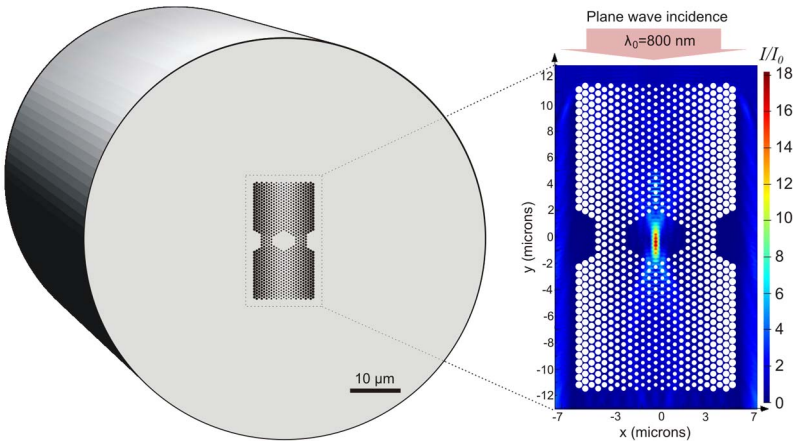

DOI: 10.1109/JPHOT.2013.2274763
1943-0655 ©2013 IEEE

IEEE photonics SOCIETY

IEEE

Photonic Crystal Mikaelian Lenses and Their Potential Use as Transverse Focusing Elements in Microstructured Fibers

T. Baghdasaryan, T. Geernaert, *Member, IEEE*, H. Thienpont, *Member, IEEE*, and F. Berghmans, *Member, IEEE*

Vrije Universiteit Brussel, Brussels Photonics Team B-PHOT, 1050 Brussels, Belgium

DOI: 10.1109/JPHOT.2013.2274763

Manuscript received May 10, 2013; revised July 12, 2013; accepted July 15, 2013. Date of publication July 25, 2013; date of current version August 5, 2013. This work was supported in part by Research Foundation-Flanders (FWO), by Methusalem and Hercules Foundations Flanders, and by the COST TD1001 Action "OFSeSA." Corresponding author: T. Baghdasaryan (e-mail: tbaghdas@b-phot.org).

Abstract: We numerically studied the focusing properties of a special type of graded index photonic crystal media, i.e., the so-called photonic crystal Mikaelian lenses (PCMLs). We considered PCMLs with a varying air hole diameter and with a varying air hole pitch in hexagonal and rectangular lattices, and we compared their frequency response and polarization dependence. Our eventual objective is to design microstructured optical fibers equipped with a PCML in their cladding region adapted to allow for more efficient femtosecond laser grating inscription. Therefore, we have also evaluated the possibility of using such lenses as transverse focusing elements in microstructured optical fibers.

Index Terms: Graded index photonic crystal, photonic crystal fibers, fiber Bragg gratings.

1. Introduction

Photonic crystal structures have been a hot research topic in the last two decades and they have impacted many applications in both linear and non-linear photonics [1]. Various devices such as filters [2], lasers [3], modulators [4] and waveguides [5] that exploit the unique features of photonic crystal structures have been reported. More recently, graded photonic crystal structures have attracted increased attention owing to their unprecedented potential for controlling and manipulating light [6], [7]. Such structures have shown to enable "super-bending" of light [8] and to allow focusing of light using devices with planar geometries [9]–[14]. Focusing of an incident beam by a photonic crystal slab is made possible by varying one of the photonic crystal parameters such as the air hole radius in the direction perpendicular to the optical axis of the focusing slab. Several planar focusing structures have already been reported and the use of graded photonic crystal structures as waveguide couplers [13], as directional antennas [11] or as broadband imaging elements [12] has been evaluated.

In our paper we study a peculiar type of graded photonic crystal lens: a so called photonic crystal Mikaelian lens (PCML) [13], [14]. In a PCML, the variation of the photonic crystal lattice parameter is adapted so as to mimic a conventional gradient index Mikaelian lens [15]. We introduce an approach to design various types of PCML and we assess the focusing properties of such PCMLs with hexagonal and rectangular lattices. We also compare those PCML structures in terms of their frequency response properties.

Our eventual objective is to implement such PCMLs as transverse focusing elements in the cladding region of microstructured optical fibers (MOFs). A microstructured optical fiber is an optical

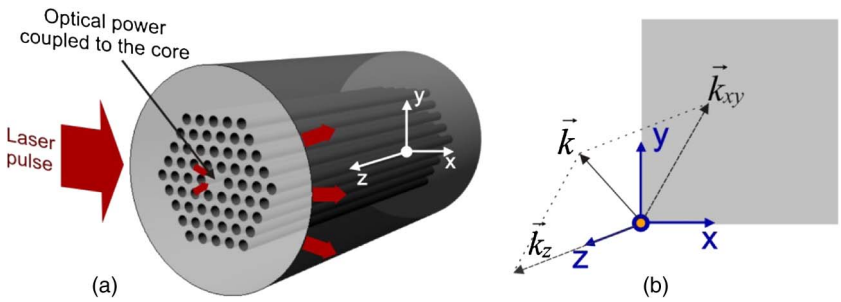

Fig. 1. Fiber transverse geometry and transverse coupling to the core, when the light propagates from the outside of the cladding through the fiber (a) and wave vector decomposition into in-plane and out-of-plane components (b).

fiber that has a transverse wavelength-scale microstructure which typically consists of air holes running along the entire length of the waveguide [16]. The unprecedented design flexibility of MOFs allows developing dedicated fibers for a variety of applications ranging from supercontinuum generation [17] and high power fiber lasers [18] to optical fiber sensors [19] as well as particle trapping in hollow core waveguides [20].

Particular attention has been paid recently to the issue of transverse light coupling to the core region of MOFs, i.e. in the direction perpendicular to the fiber length. Manipulating transversely propagating light in MOFs can have several applications. For example, all-optical switch devices based on liquid crystal filled [21] and microfluidic [22] MOFs have been proposed. A transverse beam can also be used for particle trapping experiments in hollow core fibers [20]. Understanding how light propagates through a MOF in the direction perpendicular to its axis was also found useful to investigate the structure of the MOF, to determine the angular orientation of the fiber and to analyze fiber tapers [23], [24].

Since in a MOF the array of air holes forms a photonic crystal lattice in the transverse direction of the fiber, one can conceive that implementing a PCML structure in MOFs instead of a regular array of air holes can benefit to some of the applications mentioned above. The specific application that we focus on, however, deals with improving the efficiency of fiber Bragg grating inscription in MOFs [25]. Efficient delivery of grating inscription light to the core region of a MOF is essential to enable grating formation, especially when grating formation happens during exposure to high intensity laser pulses (often femtosecond pulses) that induce refractive index modifications resulting from nonlinear multi-photon absorption processes [26].

A substantial amount of recent studies dealt with the influence of the microstructured cladding on transverse coupling of light to the core region in view of optimizing the efficiency of grating writing in MOFs [27]–[34]. We have also already tackled this issue in previous publications in which we have estimated the influence of the air hole lattice on the optical power that reaches the core of hexagonal lattice and highly birefringent MOFs [36], [37]. By doing so we were also able to show that it is possible to optimize the hexagonal lattice parameters in order to provide for enhanced transverse coupling [35]. In the current paper however, we step away from regular hexagonal lattices and we move to the PCMLs introduced above. We introduce a PCML in the cladding region with the intention to focus a transverse laser beam to the core region of the fiber. In this way we will not only overcome the detrimental influence of regular microstructured claddings on multi-photon grating writing in MOFs, but we also substantially increase the optical intensities coupled into the core region.

Before proceeding though, it is worthwhile considering the geometry of transverse coupling to the core of a MOF as illustrated in Fig. 1. Although strictly speaking, transverse pulse propagation through a MOF has a 3-dimensional nature, most of the numerical descriptions of this problem so far relied on a 2-dimensional geometry [29]–[37]. Carrying out full three-dimensional simulations of the propagation of laser pulses through a MOF requires considerable computing power, which is essentially due to the large fiber dimensions (usually diameters of 80 μm or 125 μm) compared to

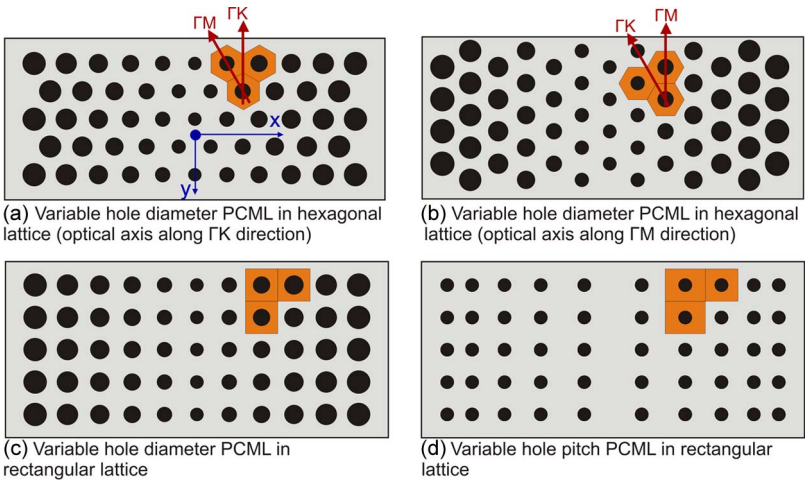

Fig. 2. Four types of photonic crystal Mikaelian lens considered in this paper. The hexagonal lattice directions (red arrows) and the primitive cells (yellow shading) are indicated.

the wavelength of light ($\sim$1 μm for infrared sources). Transverse coupling in MOFs is, however, mainly associated with the interaction of the in-plane component of the wave vector (parallel to the fiber cross-section -$\vec{k}_{xy}$), since this component interacts with the holey medium. The out of plane component of the wave vector ($\vec{k}_z$) propagates along the fiber length and the air holes, and hence does not interact with the air hole boundaries [see Fig. 1(b)]. It is therefore justified to limit the study to a two-dimensional approach. Should the transversely incident grating writing beam have an out-of-plane component (e.g. in case of oblique incidence), then our results will describe the interaction with the holey structure of the in-plane wave vector component only [1].

The rest of our paper is structured as follows: in the second section we introduce the concept of the photonic crystal Mikaelian lens (PCML), we compare different methods for designing PCMLs and we describe our approach for doing so. Section 3 deals with a comparison of four different PCML structures that have been identified as candidate structures for our target application. In Section 4 we build a MOF with a cladding region formed by the optimal PCML structure and we show how it focuses a transversely incident grating writing beam to the core region.

2. Design Methods of Photonic Crystal Mikaelian Lens (PCML)

A photonic crystal Mikaelian lens (PCML) is an implementation of a conventional Mikaelian or gradient index lens in a photonic crystal lattice. The focusing ability of a PCML structure is achieved by varying the lattice parameters: the air hole radius, the air hole pitch or the combination of both. The effective index in the PCML varies along the direction perpendicular to the optical axis according to the Mikaelian formula [15]:

$$n(x) = \frac{n_0}{\cosh(\pi x/2L)} \tag{1}$$

where n_0 is the refractive index in the center of the lens, x is the distance to the central axis of the lens and L is the lens thickness. This formula yields a focal point right in front of the structure.

We used this formula in [25], [38], where we have introduced the concept of a MOF enabling cladding assisted grating inscription, for the first time to our knowledge. At that instance we limited ourselves to a PCML with a rectangular lattice and a varying air hole radius and by doing so we only explored a limited portion of the design space. In this paper we therefore extend our study to PCMLs with hexagonal lattices and we also investigate the potential of rectangular lattice PCMLs with varying air hole pitch. This leads to a total of four possible types of PCMLs with structures illustrated in the Fig. 2.

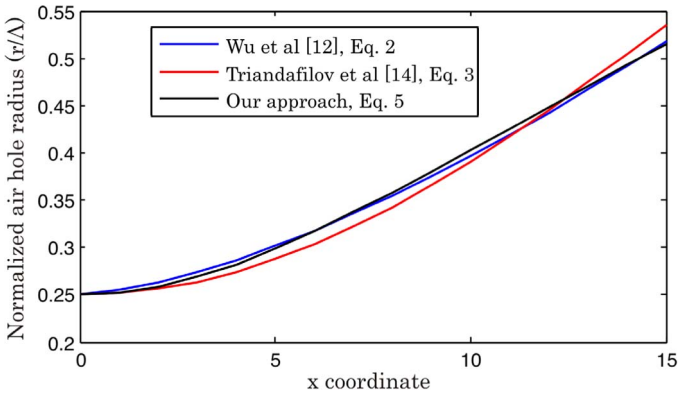

Fig. 3. Qualitative comparison of the normalized air hole radius in graded photonic crystal lens structures obtained with different calculation methods.

In order to design any graded index photonic crystal lens, we need to know the function that describes the evolution of the photonic crystal parameter in the direction perpendicular to the optical axis. Linear or quadratic functions for the variation of the air hole radius have already been reported for that purpose [9], [10]. In [12] the authors tried different grading functions for the air hole radius and compared the focusing efficiency of the resulting photonic crystal lenses. They obtained optimal focusing for an air hole radius varying as:

$$r(x)/\Lambda = 0.25 + 4.626 \cdot x^{1.4} \tag{2}$$

where Λ is the pitch of the photonic crystal lattice [12].

Triandafilov *et al.* [14] considered a rectangular PCML only and derived the air hole radii of each row from the assumption that the optical path length along the line which crosses the holes from the center should be equivalent to that of the ideal Mikaelian lens described by the Equation (1). According to [14] the air hole radius variation of a PCML should follow:

$$r(x)/\Lambda = \frac{1}{2(n-1)} \cdot \left\{ n - \frac{n_0}{\cosh(\pi x/2L)} \right\} \tag{3}$$

where n is the refractive index of the host material and n_0 is the refractive index in the center of the ideal Mikaelian lens. The main limitation of this approach is that it can be applied only to a rectangular lattice PCML with varying air hole radius and, to some extent, also to a hexagonal lattice PCML with its optical axis along the ΓM direction.

Our approach is different from those mentioned above. To calculate the air hole radius or pitch variation throughout the PCML, we considered "primitive cells", which we define in analogy to the Wigner-Seitz cell in solid-state physics [36]. The primitive cells of the four PCML types considered in this paper are illustrated in Fig. 2. The average refractive index of every primitive cell can be calculated by the following equation:

$$n_{\text{cell}} = \frac{n_{\text{air}} \cdot S_{\text{air}} + n(S_{\text{cell}} - S_{\text{air}})}{S_{\text{cell}}} \tag{4}$$

where S_{air} is the area of the air hole in a primitive cell, S_{cell} is the total area of the cell and n_{air} is the refractive index taken equal to 1 in further calculations. Taking into account Equations (1) and (4) one can derive a formula for the air hole radius variation in a rectangular lattice PCML:

$$r(x)/\Lambda = \sqrt{\left\{ n - \frac{n_{0\text{cell}}}{\cosh(\pi x/2L)} \right\} \cdot \frac{1}{\pi(n-1)}} \tag{5}$$

where n_{0cell} is the average refractive index of the primitive cell in the center of the PCML determined by the minimal air hole radius.

Fig. 3 illustrates the three grading functions given by Eqs. (2), (3), and (5). The coefficients of the equations were changed to allow for a reasonable comparison of the approaches. All three approaches give very similar results and the optimized function from [12] (Eq. (2)) is in reasonable agreement with the approach of the Mikaelian formula used by [14] (Eq. (3)) and our approach (Eq. (5)).

The advantage of our approach based on the use of primitive cells is its flexibility and its applicability to different types of PCMLs. For example and for a hexagonal lattice PCML with varying air hole radius, we can use the same reasoning as for the derivation of Eq. (5). The only difference is that the area of the primitive cell is different from that in a rectangular lattice. For a hexagonal lattice the air hole radius should vary as:

$$r(x)/\Lambda = \sqrt{\frac{\sqrt{3}}{2} \cdot \left\{ n - \frac{n_{0cell}}{\cosh(\pi x/2L)} \right\} \cdot \frac{1}{\pi(n-1)}} \tag{6}$$

which differs from Eq. (5) by a constant coefficient only. This formula can be applied to hexagonal lattice PCMLs with a gradient of the air hole radius along both the ΓK or ΓM directions.

The process of designing a PCML with a varying air hole pitch is somehow less straightforward than for a varying air hole radius. Fig. 2(d) shows that such a photonic lattice has two pitches: one along the optical axis that is constant (Λ), and one in the perpendicular direction that gradually decreases towards the edges. It is also important to note that the main parameter of the varying air hole pitch PCML is the position of the air hole or the air hole row along the x axis. To design this type of PCML we have to move row by row. For the first central row of air holes we can write the following expression for the average refractive index:

$$n_{cell\_1} = \frac{\pi r_0^2 + n\left(\Lambda \cdot 2x_1 - \pi r_0^2\right)}{\Lambda \cdot 2x_1} \tag{7}$$

where x_1 is the position and the coordinate of the first hole along the x axis, which is in fact the unknown that we aim to find. To find this unknown we require n_{cell_1} to be equal to the Mikaelian formula (1) with the corresponding coordinate; by solving this equation we can find x_1 (which can only be done numerically) and hence the position of the first air hole. Once we know the position of the first hole, we can proceed to the next. For the k-th row of air holes the equation to be solved has the following form:

$$\frac{n_0}{\cosh(\pi x_k/2L)} = \frac{\pi r_0^2 + n\left(\Lambda \cdot 2(x_k - x_{k-1} - \cdots - x_2 - x_1) - \pi r_0^2\right)}{\Lambda \cdot 2(x_k - x_{k-1} - \cdots - x_2 - x_1)} \tag{8}$$

where the unknown is x_k and where $x_{k-1}, \ldots, x_2, x_1$ are known from the previous steps.

3. Focusing Performances of Different PCML Types

We can now proceed to studying the focusing performance of the four PCMLs introduced in the previous section (see Fig. 2). Before doing so we recall a number of important issues related to the wavelength of the impinging light and we define the figure of merit that we will be working with in order to select an optimal PCML.

First and since we deal with photonic crystal structures, resonant interaction of the light with the periodic structure can affect focusing in certain wavelength ranges. Second, approximating graded index media with a photonic crystal lattice is only valid for wavelengths comparable to or smaller than the lattice features. Finally, since we intend to implement PCML structures in the cladding region of a MOF we should favor PCML structures with fairly large air holes and with relatively large lattice pitches in order for the MOF to remain manufacturable using state-of-the-art stack-and-draw or extrusion methods.

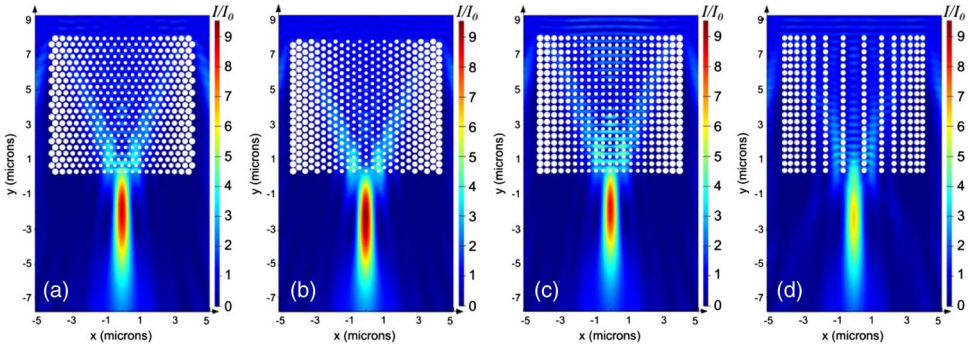

Fig. 4. Focusing of a plane wave at $\Lambda_0/\lambda = 0.33$ by 4 types of PCML structures. (a) PCML with varying air hole size in hexagonal lattice (optical axis along ΓK). (b) PCML with varying air hole size in hexagonal lattice (optical axis along ΓM). (c) PCML with varying air hole size in rectangular lattice. (d) PCML with varying air hole pitch in rectangular lattice.

To assess the focusing performance of a PCML structure in a glass MOF, we consider silica as a host material and hence we work with a material refractive index of 1.45. The maximum of the normalized intensity in the focal region I_{max}/I_0 (I_0 is the incident beam intensity) will be used for evaluating and comparing the focusing performance of the PCMLs. We compute the normalized intensity distribution across the PCML structures with the commercially available software FDTD Solutions from Lumerical Solutions Inc. [39]. I_{max} corresponds to the maximal value of the intensity found among the intensities of the pixels in the focal region. The location of the maximum intensity is therefore determined with an accuracy on the order of the mesh size (around 250 nm for 800 nm incident wavelength). In order to allow for a fair comparison of the 4 PCML types we should design PCMLs with similar overall dimensions.

We chose a reference lattice pitch of $\Lambda_0 = 400$ nm, which is half the emission wavelength of a typical laser used for multi-photon inscription of gratings, i.e. a Ti:Sapphire laser at 800 nm. In the remainder of this manuscript, all the PCML lattice features will be normalized to this reference pitch, in order for the performance analysis to be wavelength independent. We define X1 as the aperture (or the width) of the PCML and Y1 as the length (or the depth) of the PCML. The frequency of the incident light will also be normalized to the lattice pitch and will be given in dimensionless units of Λ_0/λ.

All four PCMLs were designed so as to occupy a region $X_1/\Lambda_0 = 21$ and $Y_1/\Lambda_0 = 20$. The PCML structures and their focusing performances for a TE polarized plane wave (propagating downwards from the top of the structure) are shown in the Fig. 4, in which we took the normalized frequency of the incident light $\Lambda_0/\lambda = 0.33$ for sake of illustration. In the first three PCMLs, the air hole varies from $r_1/\Lambda_0 = 0.25$ to $r_2/\Lambda_0 = 0.48$. The 4th PCML has a fixed air hole radius $r/\Lambda_0 = 0.375$ and a pitch that decreases from $\Lambda_1/\Lambda_0 = 3$ to $\Lambda_2/\Lambda_0 = 1$ in the X direction, whilst being constant in the Y direction with $\Lambda/\Lambda_0 = 1$.

Fig. 4 evidences that all four photonic crystal structures act as lenses and effectively focus incident light of this particular frequency. The normalized intensity in the focus exceeds 8 for the first three PCMLs and is slightly larger than 6 for the PCML with varying air hole pitch.

To find the PCMLs with best focusing performance we should study the normalized intensity in a broad frequency range. We therefore scanned the normalized frequency Λ_0/λ in the range from 0.2 to 1 and we computed the normalized intensity in the focus. The results are shown in the Fig. 5 for both TM and TE polarized plane wave incidence on the PCMLs.

We observe clear focusing in the low frequency region, i.e. there where the approximation of a photonic crystal lattice by a graded index medium is valid. This is also in agreement with our previous findings [38], when we compared conventional gradient lenses and PCML structures. Indeed, at low frequencies, the feature sizes of a PCML (air holes radius and/or pitch) are much smaller than the wavelength of the light, which interacts with the averaged media rather than with every individual cell. When the wavelength becomes comparable to the feature sizes of the

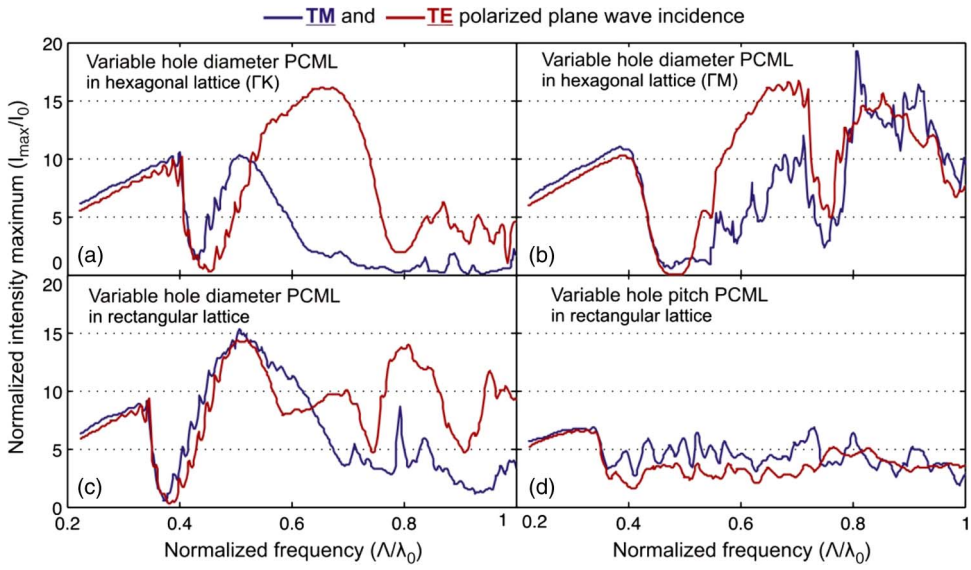

Fig. 5. Normalized intensity maximum in the focal region as a function of the normalized frequency of the incident TM and TE polarized wave for different PCML.

structure, the interaction of the light with the photonic crystal lattice is becoming more complex. This is the reason for the irregular behavior of the normalized intensity at normalized frequencies above 0.35. The abrupt decrease around a normalized frequency of 0.4 results from resonant interaction with the periodic medium and is a band gap effect. In the higher frequency region, beyond the first band gap region, the three first PCML structures again start to focus incident light, albeit with a strong dependence on the polarization.

This polarization dependence is obvious for hexagonal lattice PCMLs that exhibit notably larger focal intensities for TE polarized waves. Although the largest focal intensity is observed for TM polarized light incident on a hexagonal lattice PCML [Fig. 5(b)], this peak is very sharp and is accompanied with abrupt oscillations, indicating that such a structure would be very intolerant to manufacturing imperfections and possibly to deviations from the ideal angle of incidence between the writing beam and the microstructure. Instead, PCMLs with relatively large feature sizes that exhibit stable focusing performance over a reasonably broad frequency band can be chosen from the hexagonal lattice PCMLs, around a frequency of 0.65 for TE polarized light. A rectangular lattice PCML with varying air hole size also performs well around a frequency of 0.5 for both TM and TE polarized light.

The clear polarization dependence indicates that one could consider using PCML structures as polarization filters. This is the case, for example, for the hexagonal lattice PCML with varying air hole radius and with its optical axis along the ΓK direction, around a normalized frequency of 0.7 [see Fig. 5(a)]. This structure efficiently focuses TE light, whilst TM light scatters out of the focal region.

To close this section: with exception of the PCML with varying pitch, all the PCMLs exhibit a high focusing efficiency in a specific frequency band. A tentative explanation is that the large air hole pitch in the central part of the photonic crystal lens leads to less structuring and hence to a lower ability to harness light, compared to the varying air hole radius PCMLs. The better focusing performance of hexagonal PCMLs can be related to the fact that hexagonal photonic crystal structures can exhibit full band gaps, in contrast to rectangular structures [46].

4. PCML as Transverse Focusing Element in Microstructured Optical Fiber

As already mentioned, we aim to work with a PCML structure that has sufficiently large feature sizes, i.e. that operates in the highest possible frequency range (low wavelength range), and that

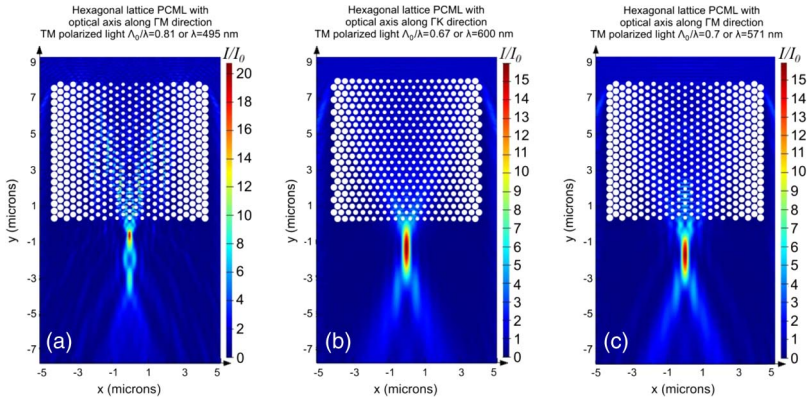

Fig. 6. Focusing performance of three PCMLs in case of plane wave incidence.

exhibits a high focusing efficiency. From Section 3, we conclude that hexagonal lattice PCMLs are best suited for that purpose.

We obtained the highest focusing efficiency in terms of the largest value of the normalized intensity for a hexagonal PCML with its optical axis along the ΓM direction and TM polarized light. Focusing of this structure at its optimal frequency is shown in Fig. 6(a). Unlike the other structures, this PCML yields a tiny focal spot in front of the lens. However, high intensity regions are also present throughout the entire PCML structure, which indicates that focusing of the incident beam is not as clean as it was for lower frequency light (see Fig. 4). The waves experience the presence of every individual hole rather than the average medium and hence the interaction of light with the holey medium is becoming more complex at those frequencies, which leads to a focusing performance that is very sensitive to changes in the incident light frequency.

Fig. 6(b) and (c) show the focusing performance of hexagonal PCMLs at their optimal frequencies of $\Lambda_0/\lambda = 0.67$ and $\Lambda_0/\lambda = 0.7$. Unlike the PCML of Fig. 6(a), they exhibit much cleaner focusing. The absence of high intensity regions throughout the PCML structure means that the approximation of the gradient structure by a holey structure remains valid. For an incident wavelength of 800 nm, which is very often used for grating inscription, the air hole pitch of the focusing structure should be around 550 nm. This is larger than the structure found in our previous study [38] for a rectangular PCML and TM polarized incident light, where we found an upper limit for the air hole pitch around 430 nm.

We can therefore use the PCML from Fig. 6(c) to design a transversely focusing microstructured fiber. The cross-section of this MOF is shown in Fig. 7(a). To design the microstructure and the core region using the PCML structure, we placed two such structures at opposite sides of the core region. The central part forms the core region and we inserted additional holes sideways to confine the guided mode in the core. The microstructure of the MOF is designed to transversely focus incident TE polarized light at 800 nm, meaning that the PCML was scaled to operate at this particular wavelength. The pitch of the PCML is 560 nm, while the air hole radius varies from 140 nm to 280 nm. The outer diameter of the MOF is chosen to be 80 μm.

Note however that there are many possible ways to design MOFs with a PCML and the design shown in Fig. 7(a) is only one of those.

The resulting MOF structure depicted in Fig. 7(a) supports a fundamental mode with a confinement loss below 0.03 dB/m. Some of the air holes where removed from the sides of the microstructure to tune the guiding properties of the fiber, which were analyzed with the commercially available software Lumerical Mode [39]. Due to the peculiar design, the MOF is birefringent with a fast axis along the *y* coordinate and a phase modal birefringence of 2×10^{-4} at 1550 nm. The normalized intensity distribution of the fundamental guiding mode is illustrated in Fig. 7(b).

Transverse focusing of an incident plane wave on the designed MOF is shown in the Fig. 8(a). The influence of the circular outer boundary of the fiber cladding was taken into account. The

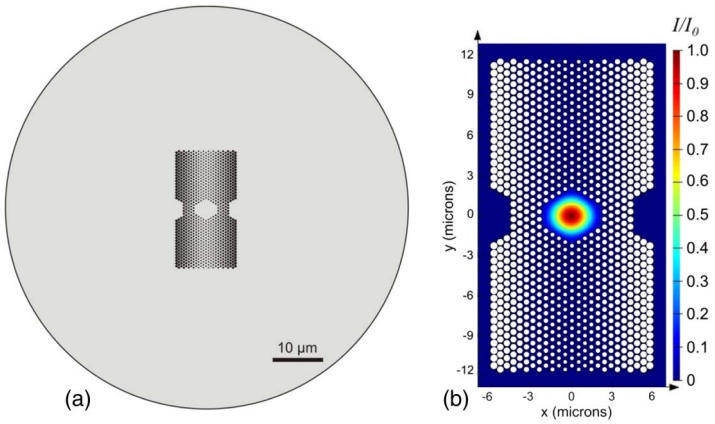

Fig. 7. Microstructured optical fiber for transverse focusing applications. (a) Design and (b) intensity profile of the fundamental mode guided by this fiber at a 1550 nm wavelength.

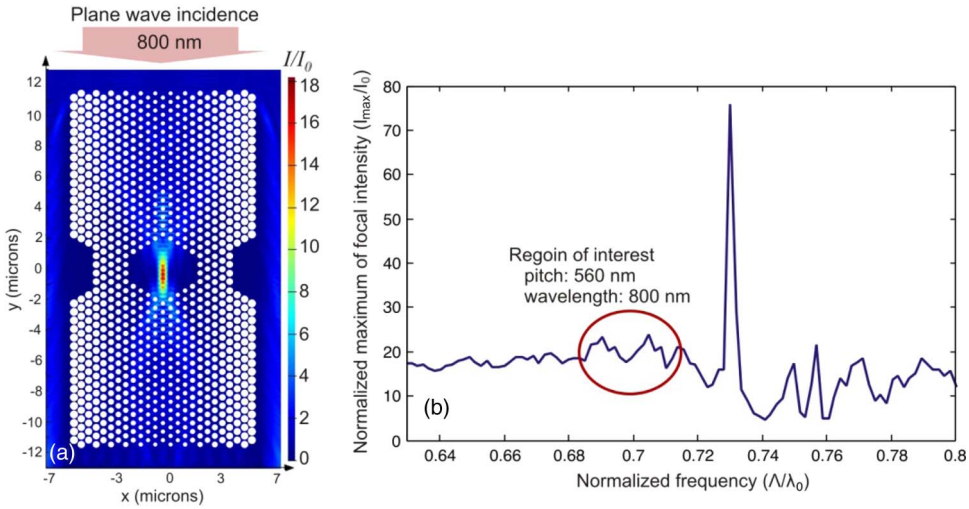

Fig. 8. (a) Transverse focusing to the core of the MOF and (b) normalized intensity maximum in the core region as a function of the normalized frequency.

incident beam is perfectly focused to the core of the fiber and the peak intensity is located in the central part of the core.

Non-linear absorption mechanism in silica during grating writing in MOFs with femtosecond lasers is not taken into account in the linear model considered in this paper. It can however cause of additional beam scattering and prohibit that the laser light reaches the core [29]. In order to avoid that such absorption would have significant impact on our results, and following the conclusions from [29], we should make sure that the intensities in the air holed cladding region are lower than the maximum focusing intensity in the core of the MOF. Our calculations depicted in Fig. 8(a) show that the maximum normalized intensity observed in the silica regions of the air holed cladding of our MOF does not exceed 5, which is 3.6 times lower than the maximum focusing intensity in the core. So we can expect that the refractive index change will truly happen in the core region, therefore ensuring a maximum overlap between the guided mode and the zone with modified refractive index.

We should also note that the transverse focusing MOFs presented here can be tuned and find applications in other domains as well. For example, relief Bragg reflectors were recently fabricated using an interference pattern that periodically etches the inner surfaces of MOF capillaries, which

were first filled with toluene [47]. The etching process is sensitive to the intensity level of the inscribing beam and by carefully designing MOFs with PCMLs it could be possible to achieve the required intensity levels in the air holed claddings near the MOF core.

The dependence of the normalized maximum intensity in the core on the incident normalized frequency is shown in Fig. 8(b). This figure essentially repeats the result shown in Fig. 5, but now takes into account the influence of the fiber cladding and the entire microstructure. In the region around $\Lambda_0/\lambda = 0.7$ (corresponding to 800 nm wavelength incidence), the maximum normalized intensity oscillates around 20, which is in accordance with our previous findings. If we consider focusing of femtosecond pulses, the bandwidth of the pulse can cover a specific frequency range depending on the pulse duration, such as indicated with a red circle in Fig. 8(b). In that case, different components of the pulse will experience various focusing conditions and here the average intensity level becomes more important than the intensity at a specific frequency.

In Fig. 8(b) we also observe a very sharp high intensity peak with a normalized intensity that reaches a value larger than 70. One should be careful when interpreting this peak and one has to take into account that we have presented results obtained with a frequency domain monitor. Such high intensities can be observed for monochromatic continuous wave incidence as a result of resonant interaction of the wave with the core region of the microstructure. For short femtosecond pulses this value can be considered as the time averaged intensity. Due to resonance the pulse can stay within the cavity formed by the fiber core and oscillate there for longer times than the duration of the pulse. This will increase the average intensity value normalized to the pulse duration, while the time domain intensity can still be on a much lower level. We have confirmed this by calculating the time and frequency domain intensities obtained for time and frequency domain monitors placed in the focal point.

Finally we have to consider the manufacturability of the MOF structure shown in Fig. 7(a). A number of reports in open literature dealt with complex microstructures that were fabricated in different materials with various air hole radii [40], [41], MOFs with a very large number of air holes [31] and MOFs with very small air hole pitches and radii [42]–[45]. We can therefore anticipate that the fabrication of our MOF design can become within reach in the near future. In our previous study [38], we designed a MOF with a PCML structure that had a pitch of 428 nm in a rectangular lattice, while here we obtained an optimal MOF structure with a pitch of 560 nm in a hexagonal lattice. This is a small, yet an important step towards a more favorable manufacturability of the structure.

5. Conclusion

We have introduced and studied four different types of photonic crystal Mikaelian lenses (PCMLs) that use either a varying air hole size in hexagonal lattices or a varying hole size and pitch in a rectangular lattice. We explained how such PCMLs can be designed starting from the Mikaelian formula and we compared our design approach to other methods that have been proposed in literature. Our method for finding adequate grading functions for the photonic crystal features has the advantage to be applicable to different types of PCMLs.

We computed the focusing performance of the different proposed PCMLs for TM and TE polarized plane waves. All 4 lenses exhibited almost identical focusing performance at normalized frequencies below $\Lambda_0/\lambda = 0.35$. However, beyond the first band gap region around $\Lambda_0/\lambda = 0.4$ the PCMLs behave differently and the maximum intensity in the focus strongly depends on the polarization of the incident light. At higher frequencies (around $\Lambda_0/\lambda = 0.7$) we observe highly efficient focusing for hexagonal lattice PCMLs and TE polarized incident light.

We applied our findings to a specific case, i.e. to the design of a microstructured optical fiber equipped with an optimized PCML in its cladding region. We simulated transverse focusing of a TE polarized wave to the core region of the fiber. The air hole pitch of the hexagonal lattice PCML used in our MOF design was 560 nm, while the air hole radius varied from 140 nm to 280 nm. The designed MOF supported a fundamental mode with a confinement loss less than 0.03 dB/m. The manufacturability of such structures still needs to be further investigated, but our simulations evidence that the MOF allows efficient delivery of light to its core region. Hence one can conceive

using such microstructures as a basis for improving the efficiency of multi-photon grating formation in structured fibers.

Implementing a photonic crystal Mikaelian lens in the cladding region of a MOF is only one of the possibilities for obtaining enhanced transverse coupling to the core for efficient femtosecond grating writing. We nevertheless hope that our work will stimulate continued work in this area and that the concept of microstructure assisted grating writing will soon be experimentally demonstrated.

References

[1] J. D. Joannopoulos, S. G. Johnson, J. N. Winn, and R. D. Meade, *Photonic Crystals: Molding the Flow of Light*. Princeton, NJ, USA: Princeton Univ. Press, 2011.

[2] Y. Akahane, T. Asano, B. S. Song, and S. Noda, "High-Q photonic nanocavity in a two-dimensional photonic crystal," *Nature*, vol. 425, no. 6961, pp. 944–947, Oct. 2003.

[3] O. Painter, R. K. Lee, A. Scherer, A. Yariv, J. D. O'brien, P. D. Dapkus, and I. Kim, "Two-dimensional photonic bandgap defect mode laser," *Science*, vol. 284, no. 5421, pp. 1819–1821, Jun. 1999.

[4] Y. Jiang, W. Jiang, L. Gu, X. Chen, and R. T. Chen, "80-micron interaction length silicon photonic crystal waveguide modulator," *Appl. Phys. Lett.*, vol. 87, no. 22, pp. 221105-1–221105-3, Nov. 2005.

[5] A. Mekis, J. C. Chen, I. Kurland, S. Fan, P. R. Villeneuve, and J. D. Joannopoulos, "High transmission through sharp bends in photonic crystal waveguides," *Phys. Rev. Lett.*, vol. 77, no. 18, pp. 3787–3790, Oct. 1996.

[6] K. V. Do, X. Le Roux, D. Marris-Morini, L. Vivien, and E. Cassan, "Experimental demonstration of light bending at optical frequencies using a non-homogenizable graded photonic crystal," *Opt. Exp.*, vol. 20, no. 4, pp. 4776–4783, Feb. 2012.

[7] K. Ren and X. Ren, "Controlling light transport by using a graded photonic crystal," *Appl. Opt.*, vol. 50, no. 15, pp. 2152–2157, May 2011.

[8] E. Centeno, D. Cassagne, and J. P. Albert, "Mirage and superbending effect in two-dimensional graded photonic crystals," *Phys. Rev. B, Condens. Matter*, vol. 73, no. 23, pp. 235119-1–235119-5, Jun. 2006.

[9] H. T. Chien and C. C. Chen, "Focusing of electromagnetic waves by periodic arrays of air holes with gradually varying radii," *Opt. Exp.*, vol. 14, no. 22, pp. 10 759–10 764, Oct. 2006.

[10] C. Tan, T. Niemi, C. Peng, and M. Pessa, "Focusing effect of a graded index photonic crystal lens," *Opt. Commun.*, vol. 284, no. 12, pp. 3140–3143, Jun. 2011.

[11] B. Vasi and R. Gajic, "Self-focusing media using graded photonic crystals: Focusing, Fourier transforming and imaging, directive emission, and directional cloaking," *J. Appl. Phys.*, vol. 110, no. 5, pp. 053103-1–053103-8, Sep. 2011.

[12] Q. Wu, J. M. Gibbons, and W. Park, "Graded negative index lens by photonic crystals," *Opt. Exp.*, vol. 16, no. 21, pp. 16 941–16 949, Oct. 2008.

[13] M. I. Kotlyar, Y. R. Triandaphilov, A. A. Kovalev, V. A. Soifer, M. V. Kotlyar, and L. O'Faolain, "Photonic crystal lens for coupling two waveguides," *Appl. Opt.*, vol. 48, no. 19, pp. 3722–3730, Jul. 2009.

[14] Y. R. Triandafilov and V. V. Kotlyar, "A photonic crystal Mikaelian lens," *Comput. Opt.*, vol. 31, no. 3, pp. 27–31, 2007.

[15] L. Mikaelian, "Harnessing medium properties for wave focusing," *Dokl. Akad. Nauk SSSR*, vol. 81, no. 2, pp. 2406–2415, 1951, (in Russian).

[16] P. Russell, "Photonic crystal fibers," *Science*, vol. 299, no. 5605, pp. 358–362, Jan. 2003.

[17] J. M. Dudley, G. Genty, and S. Coen, "Supercontinuum generation in photonic crystal fiber," *Rev. Mod. Phys.*, vol. 78, no. 4, pp. 1135–1184, Oct. 2006.

[18] M. Napierała, T. Nasiłowski, E. Bere-Pawlik, F. Berghmans, J. Wójcik, and H. Thienpont, "Extremely large-mode-area photonic crystal fibre with low bending loss," *Opt. Exp.*, vol. 18, no. 15, pp. 15 408–15 418, Jul. 2010.

[19] T. Martynkien, G. Statkiewicz-Barabach, J. Olszewski, J. Wojcik, P. Mergo, T. Geernaert, C. Sonnenfeld, A. Anuszkiewicz, M. K. Szczurowski, K. Tarnowski, M. Makara, K. Skorupski, J. Klimek, K. Poturaj, W. Urbanczyk, T. Nasilowski, F. Berghmans, and H. Thienpont, "Highly birefringent microstructured fibers with enhanced sensitivity to hydrostatic pressure," *Opt. Exp.*, vol. 18, no. 14, pp. 15 113–15 121, Jul. 2010.

[20] F. Benabid, J. Knight, and P. Russell, "Particle levitation and guidance in hollow-core photonic crystal fiber," *Opt. Exp.*, vol. 10, no. 21, pp. 1195–1203, Oct. 2002.

[21] J. Tuominen, H. Hoffrén, and H. Ludvigsen, "All-optical switch based on liquid-crystal infiltrated photonic bandgap fiber in transverse configuration," *JEOS RP*, vol. 2, p. 07016, May 2007.

[22] P. Domachuk, H. Nguyen, and B. Eggleton, "Transverse probed microfluidic switchable photonic crystal fiber devices," *IEEE Photon. Technol. Lett.*, vol. 16, no. 8, pp. 1900–1902, Aug. 2004.

[23] S. D. Lim, S. G. Lee, K. Lee, and S. B. Lee, "Determination of crystallographic axes of photonic crystal fiber by transversal scanning method," *Jpn. J. Appl. Phys.*, vol. 49, no. 10, pp. 102503-1–102503-3, Oct. 2010.

[24] L. Y. Zang, T. G. Euser, M. S. Kang, M. Scharrer, and P. St. J. Russell, "Structural analysis of photonic crystal fibers by side scattering of laser light," *Opt. Lett.*, vol. 36, no. 9, pp. 1668–1670, May 2011.

[25] F. Berghmans, T. Geernaert, T. Baghdasaryan, and H. Thienpont, "Challenges in the fabrication of fibre Bragg gratings in silica and polymer microstructured optical fibres," *Laser Photon. Rev.*, doi: 10.1002/lpor.201200103, accepted for publication.

[26] D. N. Nikogosyan, "Multi-photon high-excitation-energy approach to fibre grating inscription," *Meas. Sci. Technol.*, vol. 18, no. 1, pp. R1–R29, Jan. 2007.

[27] S. J. Mihailov, D. Grobnic, H. Ding, C. W. Smelser, and J. Broeng, "Femtosecond IR laser fabrication of Bragg gratings in photonic crystal fibers and tapers," *IEEE Photon. Technol. Lett.*, vol. 18, no. 17, pp. 1837–1839, Sep. 2006.

[28] T. Geernaert, K. Kalli, C. Koutsides, M. Komodromos, T. Nasilowski, W. Urbanczyk, J. Wojcik, F. Berghmans, and H. Thienpont, "Point-by-point fiber Bragg grating inscription in free-standing step-index and photonic crystal fibers using near-IR femtosecond laser," *Opt. Lett.*, vol. 35, no. 10, pp. 1647–1649, May 2010.
[29] T. Allsop, K. Kalli, K. Zhou, G. N. Smith, M. Komodromos, J. Petrovic, D. J. Webb, and I. Bennion, "Spectral characteristics and thermal evolution of long-period gratings in photonic crystal fibers fabricated with a near-IR radiation femtosecond laser using point-by-point inscription," *J. Opt. Soc. Amer. B, Opt. Phys.*, vol. 28, no. 9, pp. 2105–2114, Sep. 2011.
[30] G. Marshall, D. Kan, A. Asatryan, L. Botten, and M. Withford, "Transverse coupling to the core of a photonic crystal fiber: The photo-inscription of gratings," *Opt. Exp.*, vol. 15, no. 12, pp. 7876–7887, Jun. 2007.
[31] J. Holdsworth, K. Cook, J. Canning, S. Bandyopadhyay, and M. Stevenson, "Rotationally variant grating writing in photonic crystal fibres," *Open Opt. J.*, vol. 3, no. 1, pp. 19–23, Mar. 2009.
[32] J. Petrovic and T. Allsop, "Scattering of the laser writing beam in photonic crystal fibre," *Opt. Laser Technol.*, vol. 42, no. 7, pp. 1172–1175, Oct. 2010.
[33] S. Pissadakis, M. Livitziis, and G. Tsibidis, "Investigation of the Bragg grating recording in all-silica, standard and microstructured optical fibres using 248 nm, 5 ps laser radiation," *JEOS RP*, vol. 4, p. 09049, Dec. 2009.
[34] T. Geernaert, M. Becker, P. Mergo, T. Nasilowski, J. Wójcik, W. Urbanczyk, M. Rothhardt, C. Chojetzki, H. Bartelt, H. Terryn, F. Berghmans, and H. Thienpont, "Bragg grating inscription in GeO_2-doped microstructured optical fibers," *J. Lightw. Technol.*, vol. 28, no. 10, pp. 1459–1467, May 2010.
[35] T. Baghdasaryan, T. Geernaert, F. Berghmans, and H. Thienpont, "Geometrical study of a hexagonal lattice photonic crystal fiber for efficient femtosecond laser grating inscription," *Opt. Exp.*, vol. 19, no. 8, pp. 7705–7716, Apr. 2011.
[36] T. Baghdasaryan, T. Geernaert, M. Becker, K. Schuster, H. Bartelt, M. Makara, P. Mergo, F. Berghmans, and H. Thienpont, "Influence of fiber orientation on femtosecond Bragg grating inscription in pure silica microstructured optical fibers," *IEEE Photon. Technol. Lett.*, vol. 23, no. 23, pp. 1832–1834, Dec. 2011.
[37] T. Baghdasaryan, T. Geernaert, P. Mergo, F. Berghmans, and H. Thienpont, "Transverse propagation of ultraviolet and infrared femtosecond laser pulses in photonic crystal fibers," *Photon. Lett. Poland*, vol. 4, no. 2, pp. 72–74, Jun. 2012.
[38] T. Baghdasaryan, T. Geernaert, F. Berghmans, and H. Thienpont, "Microstructure-assisted grating inscription in photonic crystal fibers," *Proc. SPIE*, vol. 8426, pp. 842606-1–842606-9, 2012.
[39] [Online]. Available: http://www.lumerical.com/
[40] S. Sulejmani, C. Sonnenfeld, T. Geernaert, P. Mergo, M. Makara, K. Poturaj, K. Skorupski, T. Martynkien, G. Statkiewicz-Barabach, J. Olszewski, W. Urbanczyk, C. Caucheteur, K. Chah, P. Megret, H. Terryn, J. Van Roosbroeck, F. Berghmans, and H. Thienpont, "Control over the pressure sensitivity of Bragg grating-based sensors in highly birefringent microstructured optical fibers," *IEEE Photon. Technol. Lett.*, vol. 24, no. 6, pp. 527–529, Mar. 2012.
[41] A. Argyros, "Microstructured polymer optical fibers," *J. Lightw. Technol.*, vol. 27, no. 11, pp. 1571–1579, Jun. 2009.
[42] J. Knight, T. Birks, P. Russell, and J. Rarity, "Bragg scattering from an obliquely illuminated photonic crystal fiber," *Appl. Opt.*, vol. 37, no. 3, pp. 449–452, Jan. 1998.
[43] Y. Ruan, H. Ebendorff-Heidepriem, S. Afshar, and T. M. Monro, "Light confinement within nanoholes in nanostructured optical fibers," *Opt. Exp.*, vol. 18, no. 25, pp. 26 018–26 026, Dec. 2010.
[44] A. B. Fedotov, M. V. Alfimov, A. A. Ivanov, A. V. Tarasishin, V. I. Beloglazov, A. P. Tarasevitch, D. Von Der Linde, B. A. Kirillov, S. A. Magnitskii, D. Chorvat, D. Chorvat, Jr., A. N. Naumov, E. A. Vlasova, D. A. Sidorov-Biryukov, A. A. Podshivalov, O. A. Kolevatova, L. A. Mel'nikov, D. A. Akimov, V. A. Makarov, Y. S. Skibina, and A. M. Zheltikov, "Holey fibers with 0.4-32-um-lattice-constant photonic band-gap cladding: Fabrication, characterization, and nonlinear-optical measurements," *Laser Physics*, vol. 11, no. 1, pp. 138–145, Nov. 2001.
[45] R. Buczynski, D. Pysz, R. Stepien, R. Kasztelanic, I. Kujawa, M. Franczyk, A. Filipkowski, A. Waddie, and M. Taghizadeh, "Dispersion management in nonlinear photonic crystal fibres with nanostructured core," *JEOS RP*, vol. 6, p. 11 038, Jul. 2011.
[46] K. Ho, C. Chan, and C. Soukoulis, "Existence of a photonic gap in periodic dielectric structures," *Phys. Rev. Lett.*, vol. 65, no. 25, pp. 3152–3155, Dec. 1990.
[47] M. Konstantaki, P. Childs, M. Sozzi, and S. Pissadakis, "Relief Bragg reflectors inscribed on the capillary walls of solid-core photonic crystal fibers," *Laser Photon. Rev.*, vol. 7, no. 3, pp. 439–443, May 2013.